



Providing Choice & Value

Generic CT and MRI Contrast Agents



**FRESENIUS
KABI**

CONTACT REP

AJNR

**In Vivo X-Ray Digital Subtraction and CT
Angiography of the Murine
Cerebrovasculature Using an Intra-Arterial
Route of Contrast Injection**

G. Figueiredo, H. Boll, M. Kramer, C. Groden and M.A.
Brockmann

This information is current as
of July 11, 2025.

AJNR Am J Neuroradiol published online 10 May 2012
<http://www.ajnr.org/content/early/2012/05/10/ajnr.A3071>

ORIGINAL
RESEARCH

G. Figueiredo
H. Boll
M. Kramer
C. Groden
M.A. Brockmann

In Vivo X-Ray Digital Subtraction and CT Angiography of the Murine Cerebrovasculature Using an Intra-Arterial Route of Contrast Injection

BACKGROUND AND PURPOSE: Investigation of the anatomy, patency, and blood flow of arterial and venous vessels in small animal models of cerebral ischemia, venous thrombosis, or vasospasm is of major interest. However, due to their small caliber, in vivo examination of these vessels is technically challenging. Using micro-CT, we compared the feasibility of in vivo DSA and CTA of the murine cerebrovasculature using an intra-arterial route of contrast administration.

MATERIALS AND METHODS: The ECA was catheterized in 5 C57BL/6J mice. During intra-arterial injection of an iodized contrast agent (30 μ L/1 sec), DSA of the intra- and extracranial vessels was performed in mice breathing room air and repeated in hypoxic/hypercapnic mice. Micro-CTA was performed within 20 seconds of intra-arterial contrast injection (220 μ L/20 sec). Image quality of both methods was compared. Radiation dose measurements were performed with thermoluminescence dosimeters.

RESULTS: Both methods provided high-resolution images of the murine cerebrovasculature, with the smallest identifiable vessel calibers of ≤ 50 μ m. Due to its high temporal resolution of 30 fps, DSA allowed identification of anastomoses between the ICA and ECA by detection of retrograde flow within the superficial temporal artery. Micro-CTA during intra-arterial contrast injection resulted in a reduced injection volume and a higher contrast-to-noise ratio (19.0 ± 1.0) compared with DSA (10.0 ± 1.8) or micro-CTA when using an intravenous injection route (1.3 ± 0.4).

CONCLUSIONS: DSA of the murine cerebrovasculature is feasible using micro-CT and allows precise and repeated measurements of the vessel caliber, and changes of the vessel caliber, while providing relevant information on blood flow in vivo.

ABBREVIATIONS: ACA = anterior cerebral artery; CNR = contrast-to-noise ratio; ECA = external carotid artery; fps = frames per second; PPA = pterygopalatine artery; STA = superficial temporal artery; TS = transverse sinus

Using small animal models of human cerebrovascular diseases such as brain ischemia, venous thrombosis, or vasospasm,¹⁻⁷ researchers are able to conduct in-depth investigations of the anatomy and function of cerebral arterial, capillary, and venous vessels, which, in turn, leads to the advancement of therapeutic strategies. Due to the small caliber of murine intracerebral arteries at the base of the skull (range 100–250 μ m),^{8,9} high spatial resolutions are mandatory to allow for the analyses of anatomic and pathologic alterations of these vessels. Furthermore, the extremely short mean cerebral transit time of less than 1 second in mice¹⁰ requires sufficient temporal resolution to accurately capture information regarding intracerebral blood flow in vivo.

While micro-CTA of the cerebral vasculature in live mice is feasible at high resolutions (16 μ m)—at the expense of relatively high contrast doses (tail vein injection of 350 μ L con-

trast agent over a 40-second scan time) and high radiation doses^{9,11}—due to insufficient temporal resolution, micro-CTA and small-animal MRA¹²⁻¹⁶ do not yet allow monitoring of the murine cerebrovascular blood flow.

Nevertheless, using high temporal and spatial resolutions with synchrotron radiation-based DSA, researchers have recently reported on murine cerebrovascular blood flow^{8,13,14} and blood flow in other vessels.^{11,15,17} Because most institutions do not have easy access to a synchrotron, smaller, less expensive, and more accessible methods are preferred. For example, some researchers have implemented x-ray–based DSA of the thoracic and liver vasculature in mice.¹⁷⁻²¹ Focusing on neurovascular imaging, we found no publications describing x-ray–based DSA of the murine cerebrovasculature.

To address all of the above-mentioned limitations, we performed the underlying experiments to 1) elucidate whether high-resolution DSA of the murine cerebrovascular system is feasible without utilizing a synchrotron, and to what degree acute morphologic changes of the cerebral vessels can be identified by using such a system; 2) evaluate if contrast agent administration via an intra-arterial route allows high-contrast micro-CTA of the murine cerebrovasculature at reduced scan time and doses of contrast agent and radiation; and 3) compare both methods, focusing on the image quality of each technique.

Received October 5, 2011; accepted after revision January 23, 2012.

From the Department of Neuroradiology (G.F., H.B., C.G., M.A.B.), University of Heidelberg, Medical Faculty Mannheim, Mannheim, Germany; Department of Veterinary Clinical Sciences (M.K.), Small Animal Clinic, Justus-Liebig-University, Giessen, Germany.

The acquisition of the micro-CT (Xlon Y. Fox) was funded by the Federal Ministry of Education and Research and the Land Baden-Württemberg (HBF grant # 125–648).

Please address correspondence to Marc Brockmann, Department of Neuroradiology, Medical University Center Mannheim, University of Heidelberg, Theodor-Kutzer-Ufer 1-3, 68167 Mannheim, Germany; e-mail: brockmann@gmx.de

http://dx.doi.org/10.3174/ajnr.A3071

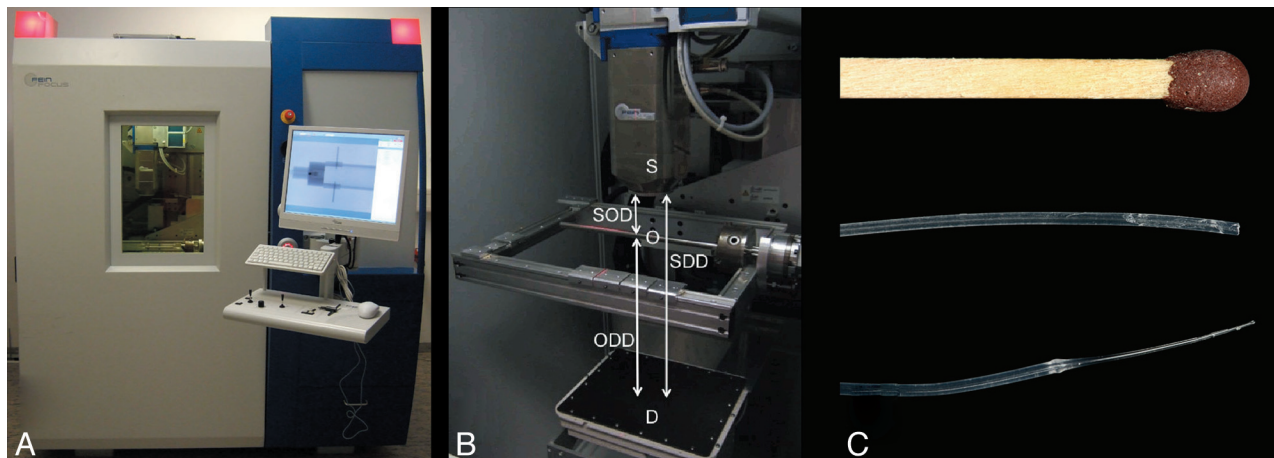


Fig 1. A, The micro-CT used for the experiments. B, A photograph of the inside of the lead-insulated cabin shows the multifocus x-ray source (S), the detector (D) beneath the x-ray source, as well as the manipulator table with the rotation axis. The height of the detector and the manipulator can be freely adjusted to optimize magnification levels that are affected by the SOD, SDD, and ODD. C, Polyethylene tubing used for intra-arterial injection of contrast agent into the external carotid artery of the mouse. To optimize the tubing system for insertion in small vessels like the ECA, the original tube (middle image; outer diameter 0.38 mm; inner diameter 0.23 mm) was tapered by applying traction to the heated tubing. The thinned polythene tube (lower image) fits well into the ECA. A matchstick (upper image) is shown for scale comparison. SOD indicates source-object distance; SDD, source-detector distance; ODD, object-detector distance.

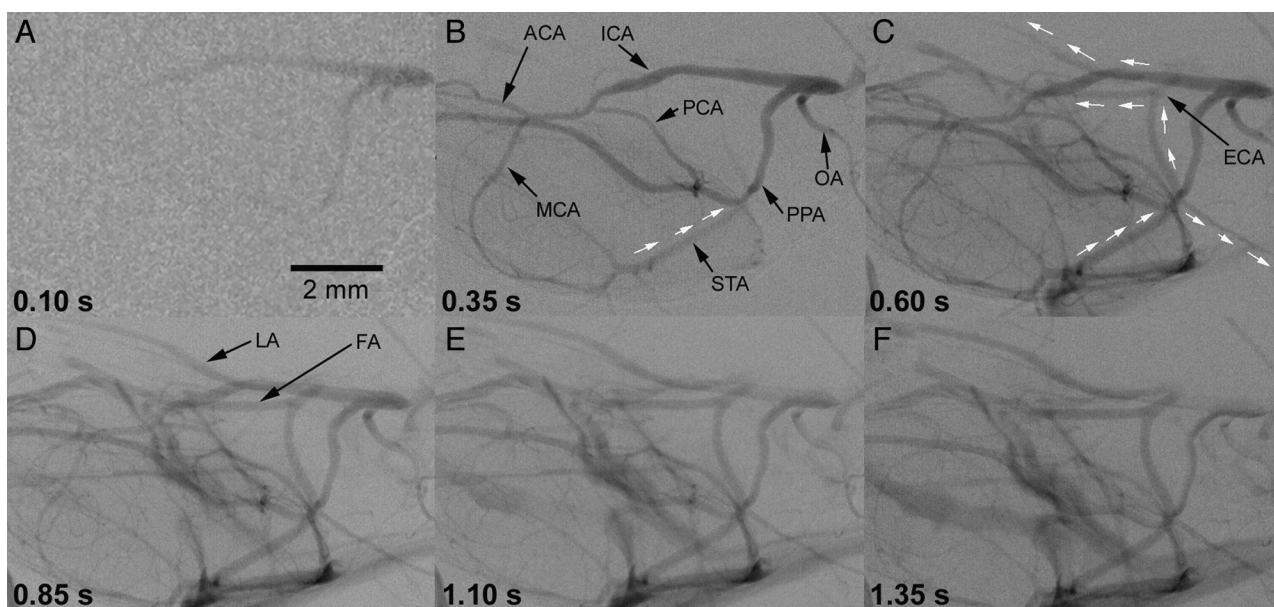


Fig 2. Cerebral DSA of a C57BL/6J mouse (craniocaudal projection). DSA (4 fps) was performed during intra-arterial injection of a bolus of 33 μ L of contrast agent within 1 second (1.980 mL/min) via the tapered polythene tubing system into the proximal ECA. The successive images show the early arterial phase (0.10 seconds and 0.35 seconds; A and B) and the parenchymal phase (0.60 seconds; C), while the veins already start to fill after 0.60 seconds (D–F). Despite ligation of the ECA during insertion of the catheter, the distal ECA and its branches are contrasted via a retrograde blood flow in the STA (white arrows in B and C) most probably via extracranial collaterals from the pterygopalatine artery. Relevant large vessels have been named to provide better orientation. PCA indicates posterior cerebral artery; OA, occipital artery; LA, lingual artery; FA, facial artery.

Materials and Methods

Animals

All experiments were carried out after receiving local ethics committee approval. Institutional guidelines for animal welfare and experimental conduct were followed. In the experiments, five 10-week-old male C57BL/6J mice, weighing 20–23 g, were used. All animals were kept in a temperature-controlled room with a 12-hour light/dark cycle and had free access to water and a standard laboratory diet.

Catheterization of the External Carotid Artery

The animals were anesthetized by intraperitoneal administration of ketamine (100 mg/kg body weight) and xylazine (5 mg/kg body weight). Using an operating microscope, the left ECA was cannulated in the retrograde direction through a small incision using a modified

polythene catheter. The catheter (Fig 1C) was prepared from polythene tubing (Portex Fine Bore Polythene Tubing; outer diameter 0.38 mm; inner diameter 0.23 mm; Smiths Medical International Ltd., Ashford Kent, United Kingdom) by heating the polythene tube for a few seconds and immediately stretching while still hot. The stretched part of the tube was cut at the thinnest section to create a catheter thin enough (outer diameter of less than 0.25 mm) to fit into the murine ECA, while still allowing injection of the contrast agent at the specified injection rates.

Digital Subtraction Angiography

An industrial micro-CT (Y. Fox; Yxlon International, Hamburg, Germany; Figs 1A and 1B) equipped with a transmission x-ray tube (Yxlon International) and an amorphous silicon flat panel detector

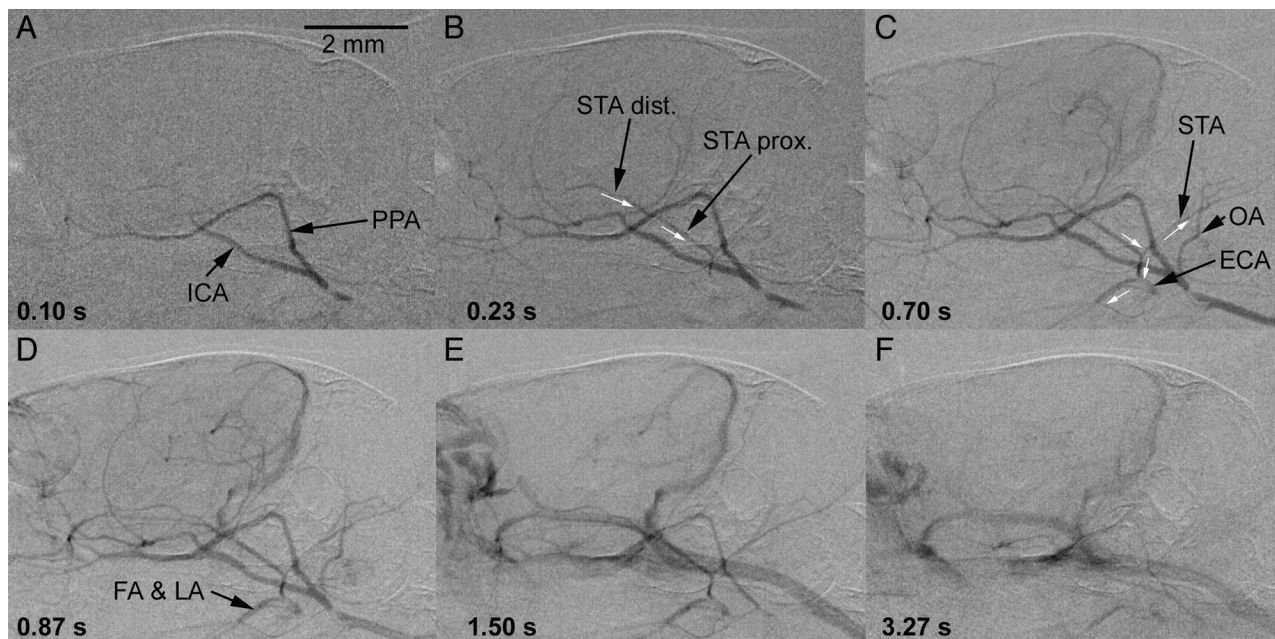


Fig 3. Cerebral DSA (30 fps) of a C57BL/6J mouse (lateral projection). High temporal and spatial resolution of the DSA again demonstrate retrograde filling of the proximally ligated ECA (A–C) via the distal and proximal rostral branch of the STA (direction of blood flow indicated by white arrows). With a slight delay, the occipital branch of the STA, as well as the FA and the LA arising from the ECA, are likewise contrasted (D). The retrograde filling occurs most likely via collaterals between the PPA and the STA. In the venous phase (E and F), the contrast of the STA diminishes from distal to proximal (once more indicating the retrograde flow), while the contrast of the FA and the LA fades away slightly later. The venous structures are shown in detail in Fig 6. FA indicates facial artery; LA, lingual artery; OA, occipital artery.

(1888 × 1408 pixels; Varian PaxScan 2520; Varian, Palo Alto, California) was used. The mouse was placed in the micro-CT and the catheter was connected to a syringe filled with prewarmed contrast agent (Iomeprol 300; Bracco Imaging, Konstanz, Germany) diluted (× 0.5) with saline solution. Using an infusion pump (PHD 2000; Harvard Apparatus, March-Hugstetten, Germany), 33 μ L of contrast agent were injected into the ECA within 1 second for cerebral DSA.

DSA was performed at 80 kV using a 2 × 2 binned detector pixel matrix of 944 × 704 at 4 and 30 fps. The tube current was maximized to optimize the SNR while preventing overexposure of the detector. The source-object distance and object-detector distance were adjusted so that the left hemisphere of the mouse filled the field of view. Gain-offset calibration was performed before contrast injection to produce DSA images (Figs 2 and 3). DSA sequences were recorded digitally in an AVI movie file format. DSA images were calibrated by performing an additional scan with a 27-gauge (0.4 mm) needle placed directly beside the animal's head at the level of the skull base.

Induction of Vessel Caliber Changes

To assess acute vessel diameter changes, each mouse underwent initial DSA in a status of normocapnia while breathing room air (time point 0'). Dilation of the cerebrovasculature was measured in a state of hypoxic hypercapnia (time point 15') by providing a gas mixture containing 5% CO₂ and 12% O₂ for 15 minutes. Finally, the animals were allowed to breathe room air again for another 15 minutes before performing the third and last DSA (time point 30').

Measurement of Vessel Calibers

Vessel caliber changes were measured using the public domain software ImageJ (v1.43u; W. Rasband, National Institutes of Health, Bethesda, Maryland). The recorded AVI files were imported and the caliber of the ICA, the MCA, and the ACA of each mouse were measured. Images of the 27-gauge needle were used for calibration. To

ensure comparable results, each vessel was measured approximately 0.5 mm proximally or distally of the bifurcation of the ICA splitting into the MCA and ACA (Fig 4). Changes of vessel diameter over time were compared using the Wilcoxon signed-rank test. A *P* value of $\leq .05$ was considered statistically significant.

Ultrafast High-Contrast Micro-CT Using Intra-Arterial Injection of Contrast Agent

Because we already had access to the arterial system after catheterization of the ECA to perform DSA, and as we were using a micro-CT system, in 2 of the animals, we subsequently tested whether micro-CT angiography within 20 seconds of continuous intra-arterial infusion of a contrast agent into the ECA yielded a sufficient image quality. The mouse was rotated over 190° during a 20-second scan time at an acquisition rate of 30 fps (600 projections; 944 × 704 pixels in a 2 × 2 binning mode; 80 kV, 75 μ A) during injection of 220 μ L of prewarmed contrast agent (Iomeprol 300 diluted × 0.5 with normal saline). Datasets were reconstructed using a filtered back-projection algorithm (Reconstruction Studio Software; Yxlon International) with Shepp-Logan filter for edge enhancement. The matrix for reconstruction was 512 × 512 × 512 voxels.

Measurement of CNR

DSA was saved in the AVI movie file format as described previously. The AVI files were imported using ImageJ and decomposed to single projections (by saving as an image sequence). The decomposed single projections were saved using the RAW file format. Eight single projections (0.033-second exposure time per projection) of the early arterial phase of each DSA were again imported in ImageJ and overlaid (opacity for each overlay set to 50%; cumulative exposure time of 0.266 seconds). The overlaid images were flattened and inverted to provide a positive vessel contrast for subsequent calculation of the CNR.

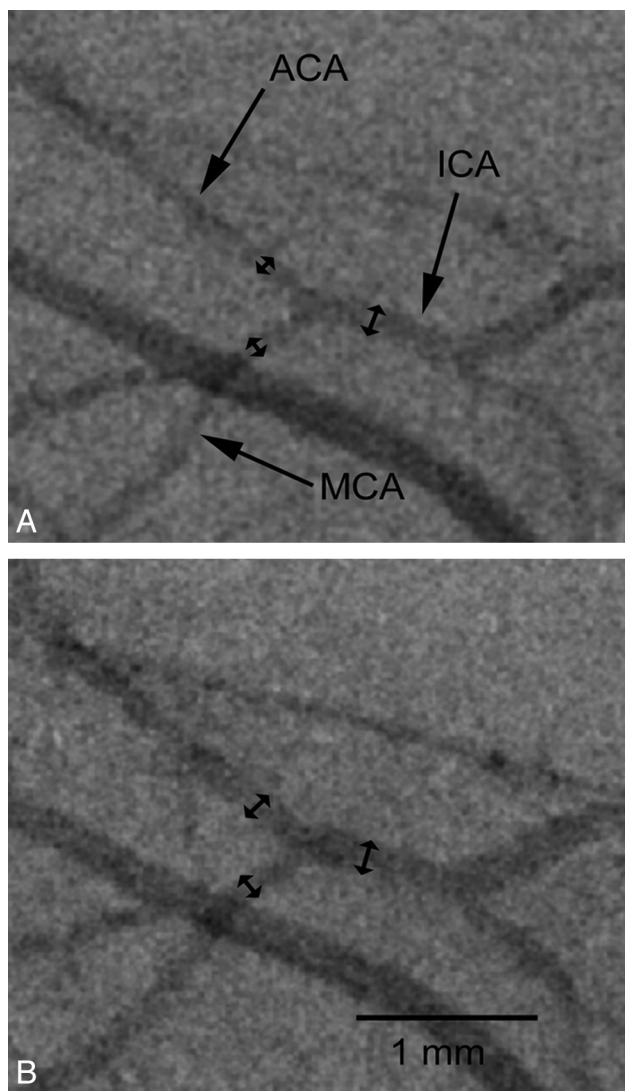


Fig 4. Repeated DSA demonstrates caliber changes of the cerebral vasculature in C57BL/6J mice. The caliber of the ICA, the MCA, and the ACA of each mouse were measured approximately 0.5 mm proximally (ICA) or distally (MCA, ACA) of the bifurcation of the ICA. *A*, DSA performed in a status of normocapnia with the animal breathing room air. *B*, After induction of hypoxic hypercapnia (5% CO₂ and 12% O₂ for 15 minutes), the cerebral vasculature is dilated.

To measure the CNR, we first determined the noise. The noise was measured as the SD of a region of interest encompassing background. Contrast was first measured by placing a region of interest within a vessel (vessel signal), and then another region of interest encompassing brain tissue (tissue signal) without discernable vessels or the ventricular system was measured. The background signal was measured by placing a region of interest in the air-filled space outside of the mouse. The tissue signal was measured as the mean image attenuation or intensity in the adjacent brain tissue. The CNR was calculated as follows:

$$\text{CNR} = \frac{\text{vessel signal} - \text{tissue signal}}{\text{SD of background signal}}.$$

Radiation Dose Measurements

Measurements of the applied radiation dose were performed by inserting a small calibrated thermoluminescence dosimeter (TLD-GR200; GC Technology, Buch am Erlbach, Germany) intra-

Table 1: Diameters (μm) of murine cerebral arteries measured in vivo using DSA

	Mouse 1	Mouse 2	Mouse 3	Mouse 4	Mouse 5	Mean \pm 1 SD	P Value
ICA							
0'	145	183	150	172	154	160.8 \pm 16.05	<.05
15'	158	210	180	178	182	181.6 \pm 18.57	
30'	122	169	138	152	140	144.2 \pm 17.50	<.05
ACA							
0'	105	143	108	112	105	114.6 \pm 16.13	<.05
15'	136	165	127	117	116	132.2 \pm 20.07	
30'	101	128	96	106	96	105.4 \pm 13.30	<.05
MCA							
0'	109	152	123	128	112	124.8 \pm 17.08	<.05
15'	116	176	145	135	120	138.4 \pm 24.03	
30'	107	131	118	126	99	116.2 \pm 13.22	<.05

Note:—Initially, DSA measurements were performed in a status of normocapnia (mice breathing room air; time point 0'). Dilatation of cerebral arteries was measured 15 minutes after induction of hypoxic hypercapnia (time point 15'). Finally, constriction of cerebral arteries was measured after breathing oxygenated room air (time point 30').

cranially (through the foramen magnum) in 2 sacrificed mice. A 20-second micro-CT scan with the above-described parameters was performed. The thermoluminescence dosimeters were sent back to the German Federal Office for Radiation Protection (Bundesamt f. Strahlenschutz, Oberschleissheim/Neuherberg, Germany) for the evaluation of the applied dose. The mean radiation dose in Gy (\pm 1 SD) was calculated.

Results

Intra-Arterial Injection of Contrast Agent

Because contrast injection may lead to nonphysiologic flow patterns, like crossflow to the contralateral hemisphere or backflow into the ICA, we analyzed the flow pattern during contrast agent injection. At the chosen flow rates of 33 $\mu\text{L}/1$ sec (DSA) and of 11 $\mu\text{L}/\text{s}$ over 20 seconds (micro-CTA) we did not observe any crossflow of contrast agent, nor did we find relevant backflow into the aortic arch. The azygos ACA, which is supplied from both proximal anterior cerebral arteries, likewise did not show sufficient contrast in DSA and micro-CTA indicative of inflow of noncontrasted blood from the contralateral anterior circulation. These observations suggest that the chosen injection rates are not strong enough to induce crossflow or relevant backflow but still provide sufficient contrast for DSA and micro-CTA, as described in the following sections. Only in 2 animals did we observe an extremely weak contrast of the ipsilateral posterior communicating and basilar artery, which is not surprising, as C57BL/6J mice are known to have a thin communicating posterior artery, which is frequently found only on 1 side.^{9,22,23} This finding may be of importance in experimental models of stroke, where stain-related differences of the vascular anatomy were related to the vulnerability of the brain and size of cerebral ischemia.

Digital Subtraction Angiography

DSA at 4 fps and 30 fps during intra-arterial injection of iodinated contrast agent into the ECA resulted in assessable images of the arterial, capillary, and venous phase of all mice. Figures 2 and 3 provide time-resolved craniocaudal and lateral DSA projections of the murine intra- and extracerebral vessels, respectively. The relevant large vessels were named to

Table 2: Comparative overview of measurement parameters of micro-CTA and DSA with intra-arterial contrast application into the ECA

	CTA _{ia}	CTA _{iv}	DSA
Number of mice	2	8	5
Scan time	20 seconds	40 seconds	~2 seconds
Radiation dose	0.25 Gy	0.5 Gy	~0.025 Gy
Contrast agent amount	220 μ L	350 μ L	33 μ L
Contrast agent concentration	lomeprol 150	lomeprol 300	lomeprol 150
Temporal resolution	>20 seconds	>40 seconds	30 fps
Spatial resolution	16 \times 16 \times 16 μ m	16 \times 16 \times 16 μ m	14 \times 14 μ m
CNR _{mean}	19.0 \pm 1.0	1.3 \pm 0.4	10.0 \pm 1.8*
Smallest detectable vessels	~50 μ m	~80 μ m	~50 μ m

* For measurement of the CNR in DSA, 8 sequentially acquired single projections were averaged. ia indicates intra-arterial; iv, intravenous.

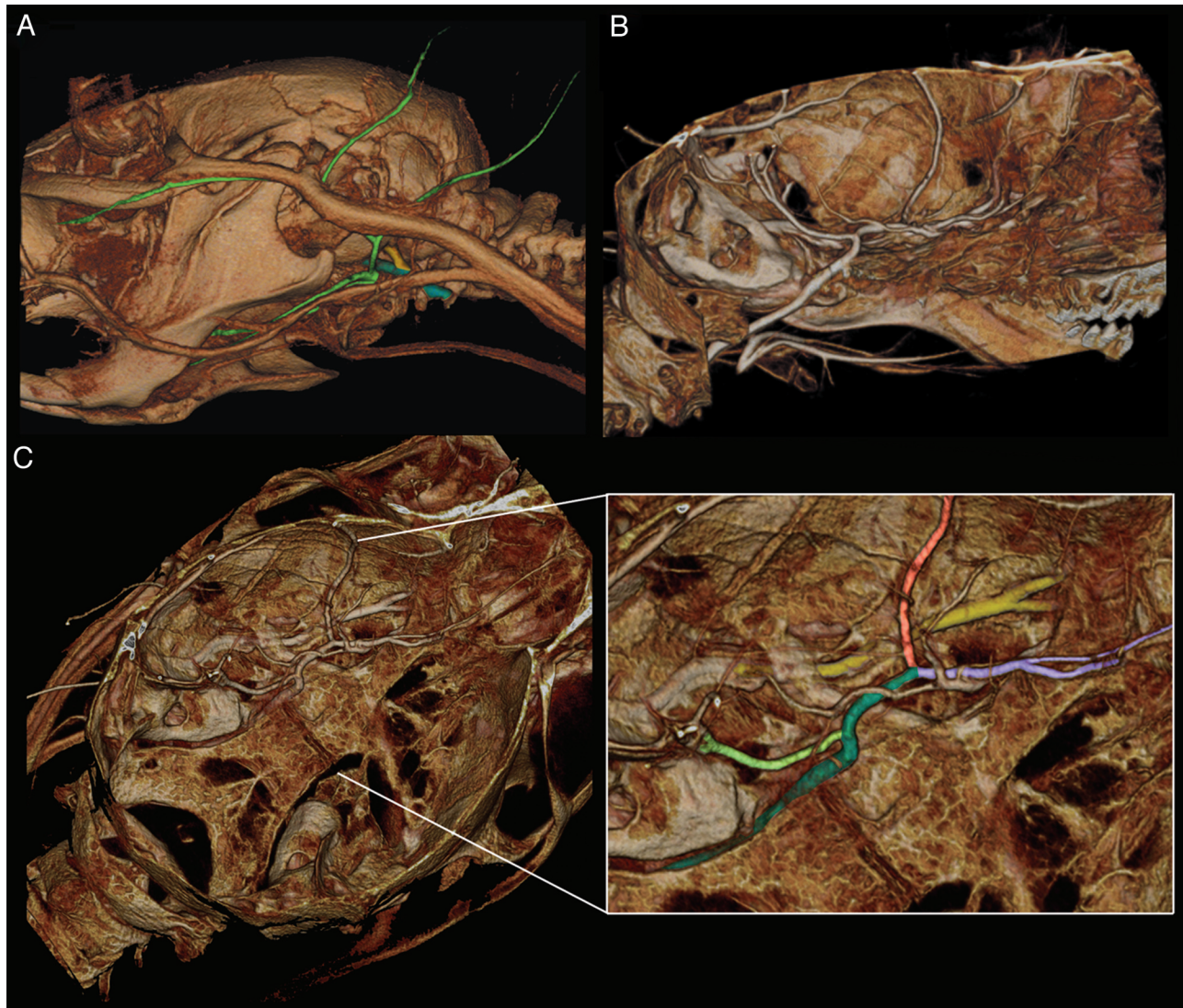


Fig 5. Volume rendering of a micro-CT angiography of a C57BL/6J mouse. Due to the relatively short mean cerebral transit time (intra-arterial injection of 220 μ L contrast media within 20 seconds scan time; 190° rotation; 600 projections; 80 kV; 75 μ As; voxel size: 39 \times 29 \times 29 μ m) the venous and the arterial vessels are superimposed. **A**, Extracranial vessels: the ICA (dark green) and the PA (yellow) both draw into the base of the skull. The branches of the ECA are colored light green, and contrast despite proximal ligation via extracranial anastomoses, as shown in the previous DSA figures. **B**, Sagittal view showing the ICA running through the base of the skull. **C**, Cranial view of the skull base showing the intracranial arteries; a close-up shows the ICA drawing through the base of the skull (dark green), as well as the PCA (light green), the MCA (light red), and the ACA (light purple), which divides into the larger azygos ACA and a smaller branch providing blood supply for the olfactory brain (better seen in the overview). Furthermore, the PA (yellow) is shown drawing along the skull base (proximal part with thin bony coverage) and dividing into a lateral and a medial branch providing, among other things, blood supply for the eye and the nasal mucosa, respectively. PA indicates pterygopalatine artery; PCA, posterior cerebral artery.

allow anatomic orientation. Although the mean cerebral transit time was not determined, the lapse of time between the initial enhancement of the ICA and filling of the larger cerebral

veins at the aforementioned injection rates was less than 1 second during DSA, which is in agreement with the literature.^{10,18} Measurements of the diameter (mean \pm 1 SD) of the proximal

MCA ($124.8 \pm 17.1 \mu\text{m}$), ACA ($114.6 \pm 16.1 \mu\text{m}$), and the distal ICA ($160.8 \pm 16.1 \mu\text{m}$) have been performed and are presented in detail for each mouse in Table 1. The smallest identifiable vessels were little cortical branches arising from the MCA with a diameter of approximately $50 \mu\text{m}$ (Fig 2C). Mean CNR of DSA was 10.0 ± 1.8 ($n = 5$ mice).

Interestingly, DSA revealed a slightly delayed contrast enhancement of the distal branches of the proximally ligated ECA in all animals, which raised the suspicion of collaterals communicating between the ICA and ECA. Assessment of DSA at 30 fps showed a retrograde flow in the STA, with subsequent enhancement of the distal ECA as well as of the facial and the lingual artery arising from the ECA. This finding is highlighted in Figs 2 and 3 (small white arrows indicate the direction of blood flow) and indicative for distal anastomoses between branches of the PPA (arising from the ICA) and the STA. Similar collaterals have also been described by Tamaki et al, who observed (in reverse order) blood flow from the ECA into the PPA after ligation of the proximal ICA.²⁴

Measurement of Vessel Diameter Changes Using DSA

Acute changes of the diameter (mean ± 1 SD) of the intracranial arteries (ICA, MCA, and ACA) were measured in 5 mice (Table 2). While breathing room air (normocapnia), the mean vessel diameter was $160.8 \pm 16.1 \mu\text{m}$ for the ICA, $114.6 \pm 16.1 \mu\text{m}$ for the ACA, and $124.8 \pm 17.1 \mu\text{m}$ for the MCA. Fifteen minutes after induction of hypoxic hypercapnia, as described, the vessel diameter increased significantly ($P < .05$ for all) to $181.6 \pm 18.6 \mu\text{m}$ (ICA), $132.2 \pm 20.1 \mu\text{m}$ (ACA), and $138.4 \pm 24.0 \mu\text{m}$ (MCA). After breathing room air again for another 15 minutes, the diameter of the cerebrovasculature decreased significantly to $144.2 \pm 17.5 \mu\text{m}$ (ICA), $105.4 \pm 13.3 \mu\text{m}$ (ACA), and $116.2 \pm 13.2 \mu\text{m}$ (MCA), respectively. Fig 4 illustrates vessel caliber changes in vivo.

Micro-CT Angiography

Although the establishment of cerebrovascular DSA in mice was the main goal of our studies and few publications describe in vivo micro-CTA in mice⁹ and rats,²⁵ we subsequently tested in 2 animals if ultrafast high-contrast micro-CT angiography is feasible. To investigate to what degree small vessels can be visualized within extremely short scan times of 20 seconds (Fig 5), contrast agent was injected through the already cannulated ECA.

The smallest identifiable vessels were the proximal branches of the retinal arteries arising from the ophthalmic artery (not shown), with the latter clearly being traceable back to the PPA. Other small vessels (diameter $< 50 \mu\text{m}$) were, for example, small muscle branches arising from the lingual artery as well as small branches arising from the MCA. From DSA, a communication between the PPA and the STA was suspected. We therefore searched for and identified very small arterial vessels located within the temporal fossa, interconnecting the STA and the PPA, explaining the almost immediate retrograde filling of the STA during DSA.

Compared to our previously published method of in vivo micro-CTA of the murine cerebrovasculature using tail-vein injection of contrast agent,⁹ we found that a better CNR could be achieved in micro-CTA (Table 2) using an intra-arterial route of contrast administration ($\text{CNR}_{\text{iv}} = 1.3 \pm 0.4$ versus

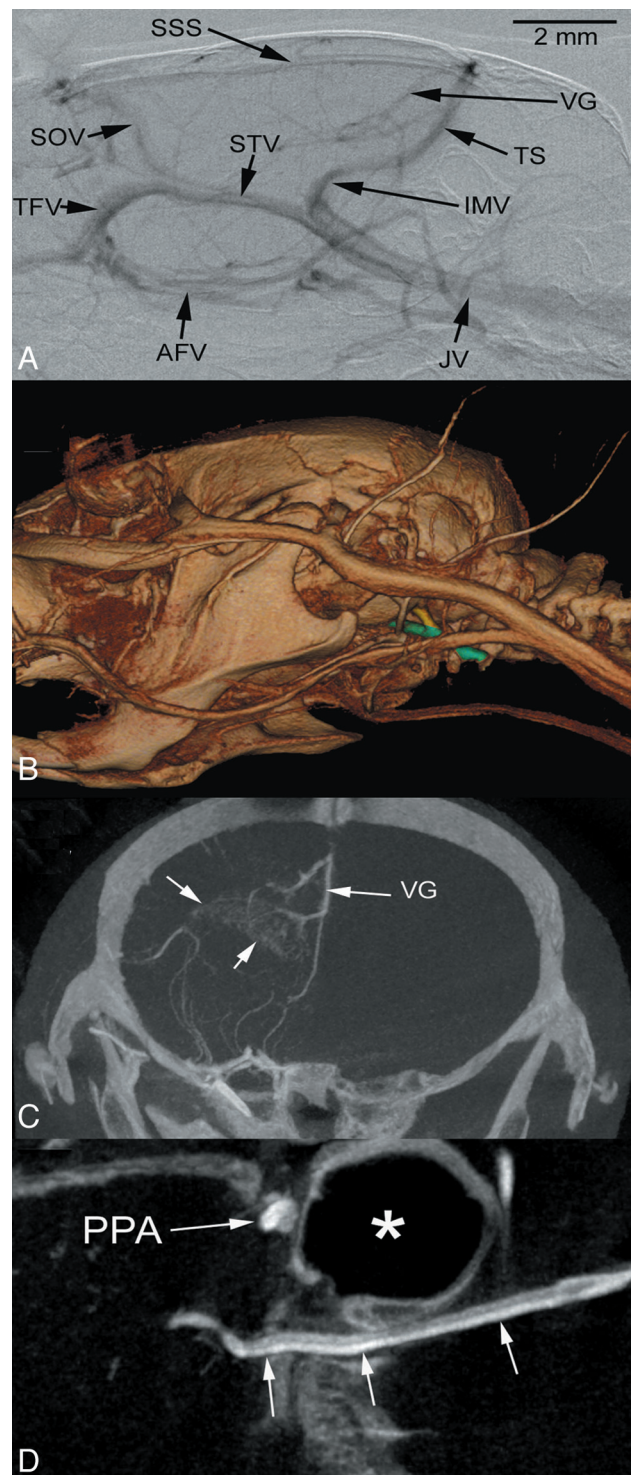


Fig 6. DSA (A, venous phase) and volume rendering of a micro-CT angiography (B), providing an overview over the intra- and extracranial venous structures. The SSS and the great cerebral vein or VG drain into the TS. The TS emerges from the cranium and is termed IMV before draining into the JV. The SOV and the TFV drain into the STV and then into the JV. The anterior facial vein drains into the JV more proximally (more clearly in micro-CT angiography images (B)). C, A coronal section (maximum intensity projection) of a micro-CT angiography shows the blush of the choroid plexus (arrows) draining into the great VG. D, Micro-CT angiography offers sufficient resolution and contrast to depict intra-arterial pathologies. As an example, dissection of the ICA (arrows), ranging from the extra- to the intracranial segment is shown. The dissection also affects the PPA (*intraosseous part is shown in close proximity to the tympanic cavity). IMV indicates internal maxillary vein; JV, jugular vein; SOV, supraorbital vein; SSS, superior sagittal sinus; STV = superficial temporal vein; TFV, transversal facial vein; TS, transverse sinus; VG, vein of Galen.

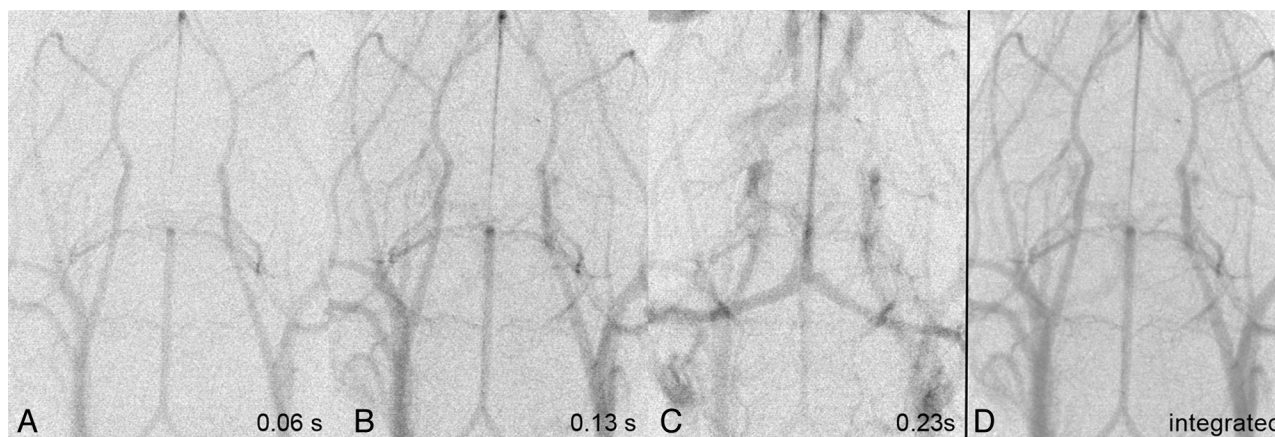


Fig 7. In vivo DSA of the murine cerebrovasculature is feasible after injection of 100 μ L Iomeprol (300 mg/L) within 1 second into the caval vein. A–C show original images acquired at 30 fps. In contrast to intra-arterial injection via the ECA, the complete circle of Willis can be assessed. D, Improved image quality after integration of 6 single images.

$\text{CNR}_{\text{ia}} = 19.0 \pm 1.0$). Furthermore, the intra-arterial injection route allowed reductions in 1) the total injection volume by 37% (350 μ L intravenous versus 220 μ L intra-arterial), 2) the contrast agent concentration by 50%, and 3) the total contrast agent dose by 70%, which is important with a total blood volume of 1.2–1.5 mL in mice. In addition, the scan time and radiation dose were halved. A disadvantage, however, was that only the cerebral vessels of 1 hemisphere could be visualized.

In addition to observing the physiologic and anatomic findings described thus far, we were also able to clearly visualize pathologic changes. In very early experiments, for example, we detected dissection of the ICA with a false and a true lumen, which was induced during the introduction of the catheter tip and which extended upward into the intracranial segment of the ICA as well as into the PPA. This finding is shown in Fig 6D and demonstrates the capability of micro-CTA to clearly visualize even subtle pathologic findings.

Radiation Dose Measurements

Radiation dose measurements using intracerebrally implanted thermoluminescence dosimeters in sacrificed mice showed a radiation dose of 0.25 ± 0.014 Gy per 20 seconds micro-CT angiography. With regard to DSA, these values can be considered as a basic value being influenced by the length and number of performed DSA procedures. In addition, the chosen source-object distance is a basic value that can be decreased to reduce the field of view, increasing the resolution of the images, as well as the locally applied radiation dose, by the inverse square law.

Discussion

With the diameter of the proximal murine cerebral arteries ranging between 100 and 200 μ m, high spatial resolutions are required to allow valid analysis of these vessels. Likewise, due to the short mean cerebral transit time of less than 1 second in mice,^{22,23,26} high temporal resolutions, which cannot be accomplished using micro-CTA, are needed to visualize and analyze the cerebral blood flow. So far, only 1 group presented useful results on the method of cerebrovascular DSA in mice.^{8,13,14,19,20} These results were obtained using a third-generation synchrotron radiation facility (SPRING 8). Advantages

of using a synchrotron are that it produces a significantly higher photon flux than conventional x-ray sources and the monochromatized x-ray energies just above the iodine K-edge energy produce the highest contrast. On the other hand, a synchrotron involves complex technology, which is costly and therefore restricted to centers with access to such a device.

As such, the main rationale for our study was to clarify whether comparable results sufficient for experimental purposes could be achieved using a conventional x-ray source, to circumvent the need for a synchrotron radiation facility to perform cerebrovascular DSA in mice.

While other groups performed in vivo x-ray DSA of liver,¹⁹ thoracic, and cerebral vessels in rats,^{11,17,18,21} and of the renal vasculature in mice,¹⁷ no studies described x-ray DSA for imaging of the cerebrovasculature in live mice. Our findings, however, demonstrate that this is highly achievable. Crucial points for successful DSA of murine cerebral vessels and the detection of vessel caliber changes are 1) a small pixel size (approximately 15 μ m in our study), 2) a sufficient contrast-to-noise ratio, which we achieved by intra-arterial administration of contrast agent, and 3) high temporal resolutions. Since superselective transfemoral catheterization of supra-aortic vessels is feasible in rats,^{11,27} but not in mice, operative cannulation of the ECA was necessary in our experiments. Thus, the use of a small catheter to fit within the ECA and the process of cannulation of the ECA were other critical steps that required some training. While trying to optimize the contrast, we experimented with different concentrations of contrast agent and found that injection of prewarmed Iomeprol 300 through the small catheter was feasible without problems, whereas the continuous injection of prewarmed Iomeprol 400 was difficult due to the exponential increase in viscosity.

While ex vivo micro-CTA of the murine cerebrovasculature has been described before,^{28,29} and fewer studies describe in vivo CTA in rats,²⁵ only 1 group, to date, has described cerebral in vivo micro-CTA in mice.^{9,11} The micro-CTA measurements presented in this manuscript differ in that 1) the scan time (and radiation dose) at 20 seconds is half as long as previously reported,⁹ 2) despite the shortened scan time, the contrast agent dose and injection volume are significantly reduced, and 3) image quality (as measured by CNR) is still superior compared with our older studies using tail-vein in-

jection. Unfavorable factors are that the unilateral approach of intra-arterial contrast administration only allows visualization of the vessels of 1 hemisphere and that catheterization of the ECA is much more invasive than tail-vein injection. Therefore, injection of a contrast agent over a catheter right into the caval vein, directly before or within the right atrium, might be an alternative to the intra-arterial approach. As we are currently investigating this alternative approach; a preliminary set of images is provided in Fig 7. The benefits to this approach are that the complete circle of Willis is contrasted and cannulation of the jugular vein is easier than that of the ECA. The vessel contrast, however, is reduced compared with the intra-arterial route.

Conclusions

We have been able to demonstrate that x-ray DSA in mice is feasible using a micro-CT system and allows measurement of changes of the diameter of the murine cerebrovasculature as well as visualization of the cerebrovascular blood flow in vivo. In addition, we demonstrated that intra-arterial administration of contrast agent allows us to perform micro-CTA in mice while reducing scan time, radiation dose, total injection volume, and contrast agent dose compared with the intravenous injection route, while still allowing the visualization of pathological lesions of the murine cerebrovasculature.

Our findings suggest that DSA and CTA of the murine cerebrovasculature are useful tools for the in vivo investigation of vascular diseases, such as vasospasm or thrombolysis, and other experimental therapeutic strategies.

References

- Barone FC, Knudsen DJ, Nelson AH, et al. Mouse strain differences in susceptibility to cerebral ischemia are related to cerebral vascular anatomy. *J Cereb Blood Flow Metab* 1993;13:683–92
- Zhang Z, Chopp M, Zhang RL, et al. A mouse model of embolic focal cerebral ischemia. *J Cereb Blood Flow Metab* 1997;17:1081–88
- Kim DE, Schellingerhout D, Jaffer FA, et al. Near-infrared fluorescent imaging of cerebral thrombi and blood-brain barrier disruption in a mouse model of cerebral venous sinus thrombosis. *J Cereb Blood Flow Metab* 2005;25:226–33
- Nagai M, Yilmaz CE, Kirchhofer D, et al. Role of coagulation factors in cerebral venous sinus and cerebral microvascular thrombosis. *Neurosurgery* 2010;66:560–65; discussion 565–66
- Sabri M, Jeon H, Ai J, et al. Anterior circulation mouse model of subarachnoid hemorrhage. *Brain Res* 2009;1295:179–85
- Sabri M, Ai J, Knight B, et al. Uncoupling of endothelial nitric oxide synthase after experimental subarachnoid hemorrhage. *J Cereb Blood Flow Metab* 2011;31:190–99
- Parra A, McGirt MJ, Sheng H, et al. Mouse model of subarachnoid hemorrhage associated cerebral vasospasm: methodological analysis. *Neurol Res* 2002;24:510–16
- Kidoguchi K, Tamaki M, Mizobe T, et al. In vivo x-ray angiography in the mouse brain using synchrotron radiation. *Stroke* 2006;37:1856–61
- Schambach SJ, Bag S, Steil V, et al. Ultrafast high-resolution in vivo volume-CTA of mice cerebral vessels. *Stroke* 2009;40:1444–50
- Rosenblum WI. Effects of blood pressure and blood viscosity on fluorescein transit time in the cerebral microcirculation in the mouse. *Circ Res* 1970;27:825–33
- Schambach SJ, Bag S, Groden C, et al. Vascular imaging in small rodents using micro-CT. *Methods* 2010;50:26–35
- Baltes C, Radzwill N, Bosshard S, et al. Micro MRI of the mouse brain using a novel 400 MHz cryogenic quadrature RF probe. *NMR Biomed* 2009;22:834–42
- Doblas S, He T, Saunders D, et al. Glioma morphology and tumor-induced vascular alterations revealed in seven rodent glioma models by in vivo magnetic resonance imaging and angiography. *J Magn Reson Imaging* 2010;32:267–75
- Bullitt E, Lin NU, Ewend MG, et al. Tumor therapeutic response and vessel tortuosity: preliminary report in metastatic breast cancer. *Med Image Comput Assist Interv* 2006;9:561–68
- Bullitt E, Wolthuisen PA, Brubaker L, et al. Malignancy-associated vessel tortuosity: a computer-assisted, MR angiographic study of choroid plexus carcinoma in genetically engineered mice. *AJNR Am J Neuroradiol* 2006;27:612–19
- Howles GP, Ghaghada KB, Qi Y, et al. High-resolution magnetic resonance angiography in the mouse using a nanoparticle blood-pool contrast agent. *Magn Reson Med* 2009;62:1447–56
- de Lin M, Ning L, Badea CT, et al. A high-precision contrast injector for small animal x-ray digital subtraction angiography. *IEEE Trans Biomed Eng* 2008;55:1082–91
- Badea CT, Drangova M, Holdsworth DW, et al. In vivo small-animal imaging using micro-CT and digital subtraction angiography. *Phys Med Biol* 2008;53:R319–50
- Lin MD, Samei E, Badea CT, et al. Optimized radiographic spectra for small animal digital subtraction angiography. *Med Phys* 2006;33:4249–57
- Lin M, Marshall CT, Qi Y, et al. Quantitative blood flow measurements in the small animal cardiopulmonary system using digital subtraction angiography. *Med Phys* 2009;36:5347–58
- Badea CT, Hedlund LW, De Lin M, et al. Tomographic digital subtraction angiography for lung perfusion estimation in rodents. *Med Phys* 2007;34:1546–55
- Rosenblum WI. Erythrocyte velocity and fluorescein transit time in the cerebral microcirculation of macroglobulinemic mice: differential effect of a hyperviscosity syndrome on the passage of erythrocytes and plasma. *Microvasc Res* 1971;3:288–96
- Rosenblum WI. Erythrocyte velocity and fluorescein transit time through the cerebral microcirculation in experimental polycythemia. *J Neuropathol Exp Neurol* 1972;31:126–31
- Tamaki M, Kidoguchi K, Mizobe T, et al. Carotid artery occlusion and collateral circulation in C57Black/6J mice detected by synchrotron radiation microangiography. *Kobe J Med Sci* 2006;52:111–18
- Seo Y, Hashimoto T, Nuki Y, et al. In vivo microCT imaging of rodent cerebral vasculature. *Phys Med Biol* 2008;53:N99–107
- Rosenblum WI. Red cell velocity and plasma transit time in the cerebral microcirculation of spherocytic deer mice. *Circ Res* 1976;39:452–54
- Buhalog A, Yasuda R, Consigny D, et al. A method for serial selective arterial catheterization and digital subtraction angiography in rodents. *AJNR Am J Neuroradiol* 2010;31:1508–11
- Abruzzo T, Tumialan L, Chaalala C, et al. Microscopic computed tomography imaging of the cerebral circulation in mice: feasibility and pitfalls. *Synapse* 2008;62:557–65
- Dorr A, Sled JG, Kabani N. Three-dimensional cerebral vasculature of the CBA mouse brain: a magnetic resonance imaging and micro computed tomography study. *Neuroimage* 2007;35:1409–23